Journal of Alloys and Compounds 508 (2010) L9–L12

Contents lists available at ScienceDirect

Journal of Alloys and Compounds

journal homepage: www.elsevier.com/locate/jallcom

Letter

TL behavior of $Ca_{0.5}Sr_{0.5}S$:Ce nanophosphors

Geeta Sharma[a,*], S.P. Lochab[b], Nafa Singh[a]

[a] Department of Physics, Kurukshetra University, Kurukshetra 136 119, India
[b] Inter University Accelerator Center, Aruna Asaf Ali Marg, New Delhi 110067, India

ARTICLE INFO

Article history:
Received 14 June 2010
Received in revised form 17 July 2010
Accepted 27 July 2010
Available online 19 August 2010

Keywords:
Mixed lattice
Nanophosphors
Luminescence

ABSTRACT

$Ca_{0.50}Sr_{0.50}S$:Ce nanophosphors were synthesized via solid state diffusion method. XRD shows a single cubic phase of $Ca_{0.50}Sr_{0.50}S$:Ce with an average size of 31 nm. TEM shows rod like structures of diameter in the range 20–30 nm and having length of several nanometers. The thermoluminescence behavior of $Ca_{0.50}Sr_{0.50}S$:Ce nanophosphors have been investigated in the low (0.1–126 Gy) and high dose (1–6 kGy) range of gamma rays from ^{60}Co source at a heating rate of 10 K/s. The TL glow curves show a main peak at 382 K with a shoulder at 470 K and a peak of very low intensity at 573 K in low dose region. In high dose range the peak position of the 382 K peak remains unchanged while the peak at 573 K shifted to 554 K and the shoulder at 470 K has turned into a peak at 456 K. The intensities of all the three peaks have increased while moving from low to high dose region but the rise in the intensities of 554 K and 456 K peaks is so rapid that these overshoot the intensity of 382 K peak in the high dose region. The effect of different heating rates (5 K/s, 10 K/s and 15 K/s) on the TL glow curve has been investigated for the samples exposed to a dose of 1 kGy. All the samples with different Sr and Ca concentrations show different TL glow curves. The PL emission spectrum has a main peak at 496 nm with a shoulder at 551 nm which may be due to the transition among 5d–4f levels of Ce in the mixed lattice.

1. Introduction

Mixed host lattices such as $Ca_{1-x}Sr_xS$ have remained the topic of interest since long because they offer scope for new applications [1,2]. These lattices possess unique properties differing from their parent lattices. Their properties can be tuned to any color of visible spectrum using a variety of dopants. Several authors have synthesized and studied the luminescence properties of mixed host lattice of Ca and Sr with a wide range of dopants e.g. Sung et al. have studied the optical properties (PL and PLE spectra) of $Ca_{1-x}Sr_xS$:Mn [3]. Wang et al. have reported the photoluminescence behavior of $Sr_{1-x}Ca_xS$ synthesized by solvothermal method [4]. Kato et al. have studied preparation and cathodoluminescence of CaS:Eu and $Ca_{1-x}Sr_xS$:Eu phosphors [5]. Haecke et al. have also reported the influence of source powder preparation on the electroluminescence of $Ca_{1-x}Sr_xS$:Eu thin films [6]. But the reports on the thermoluminescence behavior of mixed alkaline earth sulphides are very scanty. Also it is well known that Ce acts as a very good dopant for alkaline earth sulphide phosphors [7,8]. It gives different emission colors in different hosts, making it a versatile doping material.

We have synthesized single phased $Ca_{0.5}Sr_{0.5}S$:Ce using solid state diffusion method [9] and investigated its thermoluminescence behavior for gamma exposure. The phase characterization was done by XRD, and TEM was used to study the morphology of the nanophosphors. Recently, we have reported the thermoluminescence behavior of Ce doped CaS nanoparticles exposed to gamma radiations [10] and in continuation to our previous work this paper aims at the thermoluminescence study of ^{60}Co-γ irradiated Ce doped $Ca_{0.5}Sr_{0.5}S$ nanoparticles since the addition of Sr to the CaS host made us curious to study the changes in the TL properties caused by this addition.

2. Experimental

We used solid state diffusion method for synthesizing $Ca_{0.5}Sr_{0.5}S$:Ce. Calcium sulphate, strontium sulphate, cerium nitrate, sodium thoisulphate, carbon powder and ethanol were the starting materials. Carbon reduces sulphate to sulphide at high temperature and cerium acts as an activator. Sodium thoisulphate (15%) acts as a flux for the reaction. The calculated quantities of calcium sulphate, strontium sulphate, carbon powder, cerium nitrate (0.2 mol.%) and the flux were taken and mixed thoroughly with the help of an agate pestle and mortar. The charge was placed in a clean graphite crucible and a thin layer of carbon powder was spread over it. This crucible was covered with another similar crucible. The thin layer of the carbon over the charge created a reducing environment over the charge. This whole arrangement was placed in a muffle furnace and the charge was fired at 950 °C for 2 h. After 2 h the charge was taken out and rapidly crushed while red hot with the help of a pestle and mortar. The details of the nanoparticle preparation are reported elsewhere [9].

The samples were characterized by X-ray powder diffraction (XRD) using an in situ XRD set up (Bruker AXS) having a 3 kW X-rays source. For recording TL,

* Corresponding author. Tel.: +91 9466471265.
E-mail address: g.sharma.ku@gmail.com (G. Sharma).

0925-8388/$ – see front matter © 2010 Elsevier B.V. All rights reserved.
doi:10.1016/j.jallcom.2010.07.225

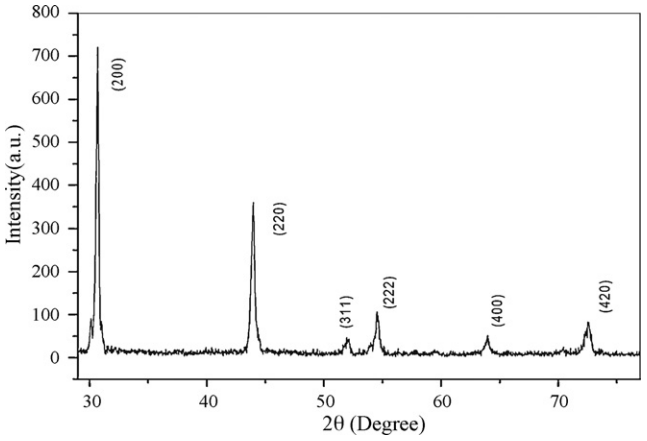

Fig. 1. XRD pattern of $Ca_{0.5}Sr_{0.5}S$:Ce.

samples were irradiated with different doses of ^{60}Co γ-rays at room temperature. Prior to gamma exposure, the samples were annealed at 400 °C for 10 min and then quenched on a metallic plate at room temperature to erase any residual information. TL glow curves were recorded on a Harshaw TLD reader (Model 3500) fitted with 931B photomultiplier tube (PMT) by taking 5 mg of sample each time.

3. Results and discussion

3.1. X-ray diffraction and TEM

Fig. 1 shows the XRD pattern for $Ca_{0.5}Sr_{0.5}S$:Ce. The XRD patterns matched perfectly with standard data available in JCPDS (75-0266), except line broadening of the diffraction peaks. No separate phases of CaS and SrS were observed which shows efficient substitution of Ca^{2+} sites by Sr^{2+} ions. The well-known Debye–Schere's [11] relation was used to estimate the particles size for Ce doped $Ca_{0.5}Sr_{0.5}S$ after correcting for instrumental broadening. The particle size was found to be 31 nm. TEM shows rod like structures with an average diameter of 20–30 nm and a length of several nanometers (Fig. 2). The inset in Fig. 2 shows the selected area diffraction pattern for $Ca_{0.5}Sr_{0.5}S$:Ce nanoparticles. Three distinct lattice reflections (2 0 0), (2 2 0) and (3 1 1) occur at interplanar spacing, d_{hkl} of 0.31 nm, 0.20 nm and 0.15 nm respectively. The particles size estimation from TEM and XRD studies were found to be in close agreement.

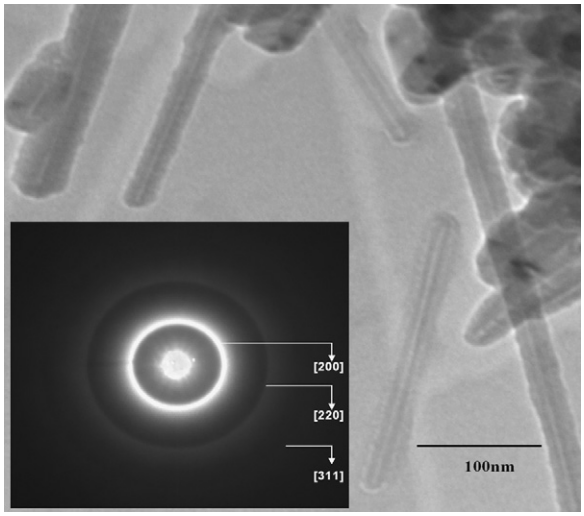

Fig. 2. TEM image of $Ca_{0.5}Sr_{0.5}S$:Ce. Inset in the figure shows the SAED pattern of the nanoparticles.

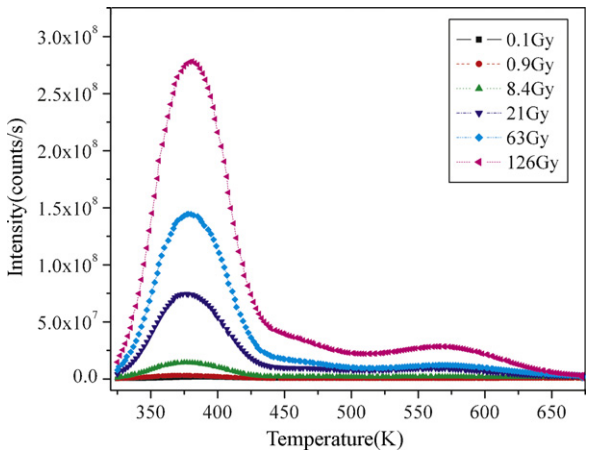

Fig. 3. TL glow curves of $Ca_{0.5}Sr_{0.5}S$:Ce at low dose range (0.1–126 Gy) of gamma rays from ^{60}Co source at a heating rate of 10 K/s.

3.2. Thermoluminescence characteristics

We have investigated the effect of different doses of gamma on the TL glow curves of $Ca_{0.5}Sr_{0.5}S$:Ce nanoparticles. The glow curves show different TL behaviors at the low and relatively higher dose range. A similar behavior was also observed by Vij et al. for gamma exposed Ce doped SrS nanostructures [12]. Fig. 3 shows the TL glow curves of $Ca_{0.5}Sr_{0.5}S$:Ce at low dose range (0.1–126 Gy) of gamma rays from ^{60}Co source at a heating rate of 10 K/s. The glow curve has a main peak at 382 K with a shoulder at 470 K and a peak of very low intensity at 573 K. With increasing dose the intensity of both the low and the high temperature peaks increases but the peak positions remain unchanged.

Fig. 4 shows the variation in TL intensity of the main peak (382 K) with increasing dose. The TL intensity increases almost linearly with increasing dose. This linear behavior with the dose is also important from the dosimeteric point of view and hence this peak can be used as a dosimeteric peak for this dose range.

TL glow curves for the samples exposed in the range 1–6 kGy were surprisingly different. Glow curves for high dose regime are shown in Fig. 5. The TL glow curves comprise of three peaks, a strong peak around 554 K and two relatively less intense peaks around 456 K and 382 K. There is a variation in the peak positions with the variation in the dose. Some authors have also reported such shifts in the TL peak position with ion beam bombardment and

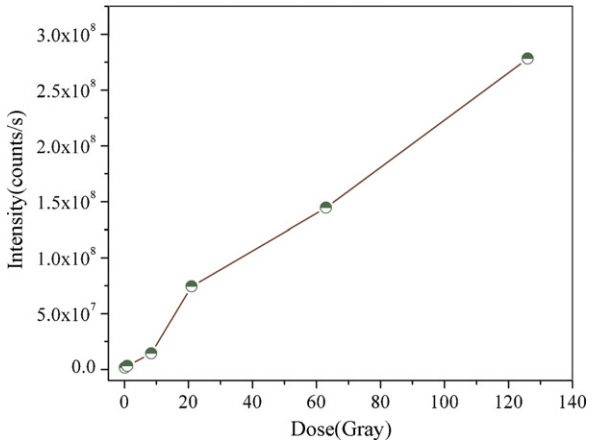

Fig. 4. Variation of TL intensity of the 381 K peak with increasing dose in low dose region.

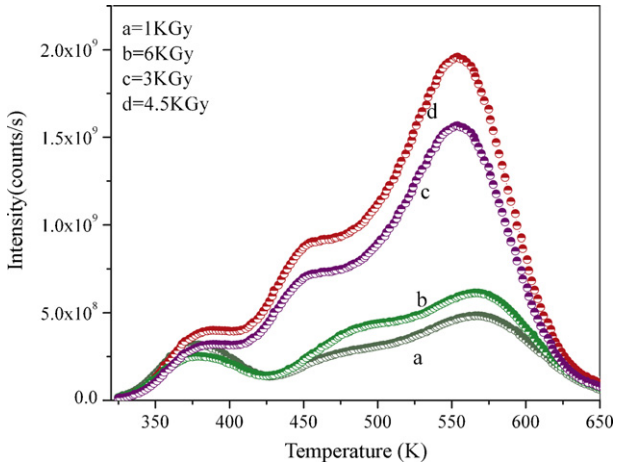

Fig. 5. Glow curves of $Ca_{0.5}Sr_{0.5}S$:Ce for high dose regime (1–6 kGy).

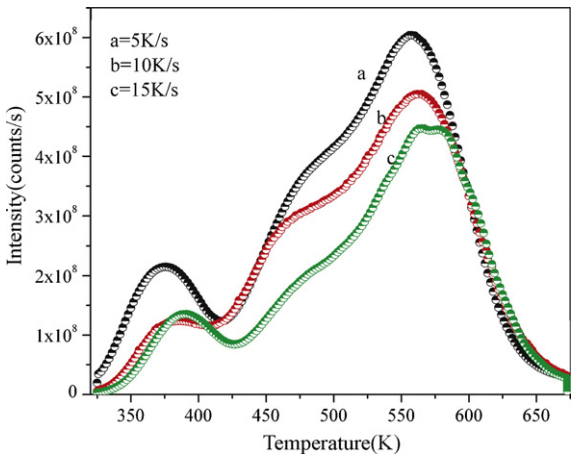

Fig. 7. Influence of different heating rates on TL glow curve of $Ca_{0.5}Sr_{0.5}S$:Ce (exposed to 1 kGy of gamma rays).

attributed this effect to disorganization of the initial energy bands [13,14].

A comparison between the TL glow curves in the low and high dose range shows that the peak position of the 382 K peak remains unchanged in both the regions while the peaks at 573 K shifted to 554 K and the shoulder at 470 K has turned into a peak at 456 K in the high dose range. Besides the variation in the peak positions the change in the intensities of the peaks is also surprising. In the low dose range the peak at 382 K has remained the most intense peak and the other two peaks were very less intense but on the other hand in the high dose range the peak around 554 K is having the maximum intensity and 382 K peak is the least intense. The intensities of all the three peaks have increased while moving from low to high dose range but the rise in the intensities of 554 K and 456 K peak is so rapid that these overshoot the intensity of 382 K peak in the high dose range. Different behaviors in the two dose ranges indicates that high dose of gamma might be forming some deep traps in the host lattice hence giving a rapid rise to the peak intensities at 554 K and 456 K. The intensities of all the three peaks increase up to 4.5 kGy dose in the high dose regime and afterwards a fall is recorded with further increase in the dose. Variation in the intensities of the 382 K peak and 554 K peak in the high dose range is shown in the Fig. 6. It is clear from the figure that intensity of 382 K peak rises gradually while there is a rapid and linear rise in the intensity of 544 K peak up to 4.5 kGy. This linear behavior over a wide range of dose in nanocrystalline materials can be explained on the basis of TIM [15,16] and their high surface to volume ratio. According to this model, the number of traps generated by the high energy radiation in a track depends upon the cross-section and the length of the track inside the matrix. In case of nanomaterials the length of the track generated by high energy radiation is of the order of a few tenths of nanomaterials. At low doses there exist a few trap centers (TC)/luminescent centers (LC). As the dose increases, the TL intensity increases as still some particles exist that would have missed while being targeted by the high energy radiation, owing to the small size of the particles. This gives good linearity over a wide range of dose. The effect of different heating rates on the TL glow curve has been investigated for the samples exposed to a dose of 1 kGy which is shown in Fig. 7. We noted that as we increase the heating rate from 5 K/s to 15 K/s, TL intensities decrease with a shift in the peak to a higher temperature which is in agreement with our previous results [10]. This may be assigned to the well-known thermal quenching of TL due to an increase in heating rates.

Thermoluminescence characteristics of ^{60}Co irradiated $Ca_{0.25}Sr_{0.75}S$:Ce and $Ca_{0.75}Sr_{0.25}S$:Ce have also been investigated. Fig. 8 shows the TL glow curve for $Ca_{1-x}Sr_xS$:Ce exposed to 6 kGy of ^{60}Co gamma rays. All the three glow curves possess different shapes. For $Ca_{0.25}Sr_{0.75}S$:Ce, TL glow curve consists of a low intensity peak at 393 K with a main broad peak at 494 K. The TL glow curve for $Ca_{0.50}Sr_{0.50}S$:Ce comprises of a main peak at 566 K along with two shoulders at 380 K and 492 K. The glow curve for $Ca_{0.75}Sr_{0.25}S$:Ce possess a simple shape with a main broad peak at

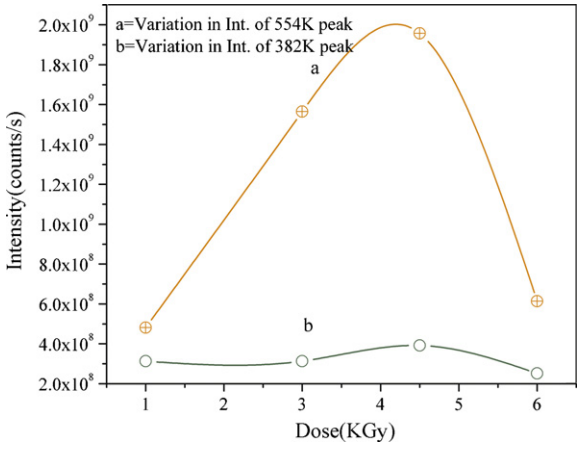

Fig. 6. Variation in the intensities of the 382 K peak and 554 K peak in the high dose range.

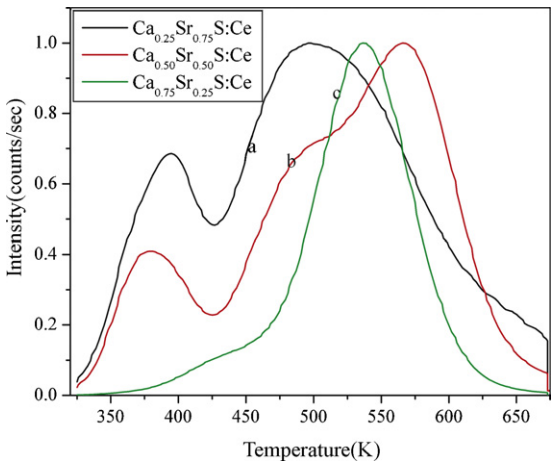

Fig. 8. TL glow curve for $Ca_{1-x}Sr_xS$:Ce exposed to 6 kGy of ^{60}Co gamma rays.

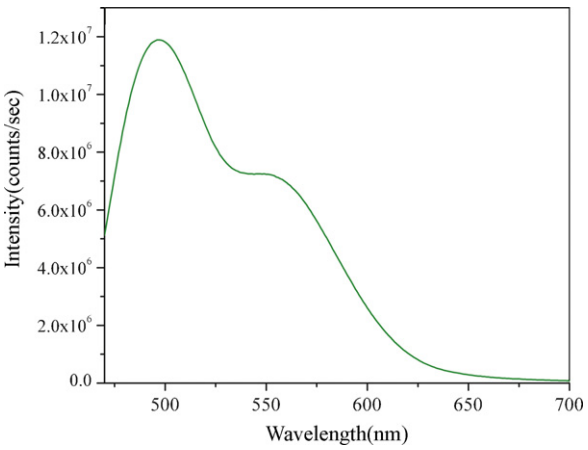

Fig. 9. PL emission spectrum of $Ca_{0.5}Sr_{0.5}S$:Ce at an excitation wavelength of 450 nm.

536 K and a very low intensity peak at 430 K. Hence the variation of Ca and Sr contents lead to change in the defect structure of the host lattice resulting in a change in the shape of glow curves.

A comparison of TL glow curves of CaS:Ce from our previous study [10] and $Ca_{0.5}Sr_{0.5}S$:Ce shows that glow curve for CaS:Ce have two peaks, one around 400 K and a high temperature peak at 560 K. With increasing dose the intensities of both the peaks increase but there is a rapid rise in the intensity of the high temperature peak. While $Ca_{0.5}Sr_{0.5}S$:Ce show three peaks which vary in intensity and peak positions with increasing dose of gamma. One peculiar similarity between the two cases is that at low doses the low temperature peak is more intense and with increasing dose the intensity of high temperature peak increases. The addition of Sr might have incorporated some new defects in the host lattice.

3.3. Photoluminescence characteristics

The PL spectrum of $Ca_{0.5}Sr_{0.5}S$:Ce nanoparticles have been recorded. Fig. 9 shows the emission characteristics of $Ca_{0.5}Sr_{0.5}S$:Ce at an excitation wavelength of 450 nm. The emission spectrum consists of a main peak at 496 nm with a shoulder at 551 nm. These peaks may be attributed to the well-known 5d–4f transitions of Ce. The 4f ground state of Ce^{3+} splits to two levels $^2F_{7/2}$ and $^2F_{5/2}$ as a result of spin–orbit coupling [17]. The excited state 5d of Ce^{3+} is sensitive to crystal field and thus splits into a doublet E_g and a triplet T_{2g} level with T_{2g} at a lower energy. Therefore, the peak at 496 nm and the shoulder at 551 nm may be attributed to the transitions from the T_{2g} sublevel of the 5d excited state to $^2F_{5/2}$ and $^2F_{7/2}$ of the 4f ground state of Ce^{3+} [18].

4. Conclusions

$Ca_{0.5}Sr_{0.5}S$:Ce nanoparticles were synthesized via solid state diffusion method. XRD and TEM were used to study the size and structure of the nanoparticles. The thermoluminescence behavior of $Ca_{0.50}Sr_{0.50}S$:Ce nanophosphor has been investigated in the low (0.1–126 Gy) and high dose (1–6 kGy) regime. The glow curves show three peaks in both the regimes, but the intensities and the peak positions vary in the two regions which might be due to the deep traps formed in the host lattice at high doses. With increasing heating rates the glow peaks shift towards higher temperature side and their intensities fall due to the phenomenon of thermal quenching as a result of increase in the heating rate. The shapes of the TL glow curve for $Ca_{1-x}Sr_xS$:Ce (x = 0.25, 0.50, 0.75) exposed to 6 kGy of ^{60}Co gamma rays are different from each other indicating variation of Ca and Sr contents.

Acknowledgement

One of the authors GS is thankful to I.U.A.C., New Delhi for financial help in the form of a fellowship under the UFUP-44305 project.

References

[1] J. Zhang, J. Wang, R. Yu, H. Yuan, Q. Su, Mater. Res. Bull. 44 (2009) 1093–1096.
[2] Q. Xia, M. Batentschuk, A. Osvet, A. Winnacker, J. Schneider, Radiat. Meas. (2009), doi:10.1016/j.radmeas.2009.09.010.
[3] H.J. Sung, Y.D. Huh, Korean J. Mater. Res. 17 (2007) 137–141.
[4] C. Wang, K. Tang, Q. Yang, Y. Qian, J. Electrochem. Soc. 150 (2003) G163–G166.
[5] K. Kato, F. Okamoto, Jpn. J. Appl. Phys. 22 (1983) 76–78.
[6] J.E. Van Haecke, P.F. Smet, D. Poelman, Spectrochim. Acta B 59 (2004) 1759–1764.
[7] A. Vedda, N. Chiodini, D. Di Martino, M. Fasoli, S. Keffer, A. Lauria, M. Martini, F. Moretti, G. Spinolo, M. Nikl, N. Solovieva, G. Brambilla, Appl. Phys. Lett. 85 (2004) 6356–6358.
[8] W.L. Warren, K. Vanheusden, C.H. Searger, D.R. Tallant, J.A. Tuchman, S.D. Silliman, D.T. Brower, J. Appl. Phys. 80 (1996) 12.
[9] G. Sharma, P. Chawla, S.P. Lochab, N. Singh, Radiat. Eff. Defects Solids 164 (2009) 763–770.
[10] G. Sharma, S.P. Lochab, N. Singh, J. Alloys Compd. 501 (2010) 190–192.
[11] B.D. Cullity, Elements of X-ray Diffraction, Addison-Wesley, London, 1959.
[12] A. Vij, S.P. Lochab, R. Kumar, N. Singh, J. Alloys Compd. 490 (2009) L33–L36.
[13] J. Gaikwad, S. Thomas, S. Kamble, P.B. Vidyasagar, A. Sarma, Nucl. Instrum. Methods B 156 (1999) 231–235.
[14] N. Salah, P.D. Sahare, J. Phys. D: Appl. Phys. 39 (2006) 2684.
[15] S. Mahajna, Y.S. Horowtz, J. Phys. D: Appl. Phys. 30 (1997) 2603.
[16] Y.S. Horowitz, O. Avila, M. Rodrigues-Villafuerte, Nucl. Instrum. Methods Phys. Res. B 184 (2001) 85–112.
[17] Z. Wang, M. Xu, W. Zhang, M. Yin, J. Lumin. 122 (2007) 437–439.
[18] D. Jia, R.S. Meltzer, W.M. Yen, J. Lumin. 99 (2002) 1–6.